



ISSN: 2468-0230

Surfaces and Interfaces

[Elsevier Physics homepage](#)Publishing options:  Open Access [↗](#)  Subscription [↗](#)[↗ Guide for authors](#) [Track your paper](#) [Submit your paper](#)

The Impact Factor of this journal is 4.837, ranking it 4 out of 21 in *Materials Science, Coatings & Films*



With this journal indexed in 2 international databases, your published article can be read and cited by researchers worldwide

[View articles](#)

Editors > Editorial board

Dr. Mihaela Baibarac, PhD, Prof. Mircea Chipara, PhD, Prof. Dr. Hong Deng, PhD, Prof. Dr. Jinwei Gao, PhD, Prof. Zhenping Qu, PhD, Dr. Klaus Zimmer, PhD...

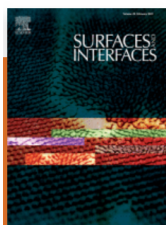
The journal *Surfaces and Interfaces* publishes new, original, up to date, and scientifically interesting topics in all research areas on surfaces and interfaces.

The journal aims at being a fast and efficient platform for disseminating scientific results in this wide area of research. Fundamental, interdisciplinary, theoretical, experimental and applied work will be considered.







ScienceDirect

Journals & Books

 [Register](#)[Sign in](#)

Surfaces and Interfaces

4.8
CiteScore4.837
Impact Factor[Articles & Issues](#) [About](#) [Publish](#) [Order journal](#)  [Search in this journal](#)[Submit your article](#) [Guide for authors](#) 

Volume 28

February 2022

[< Previous vol/issue](#)[Next vol/issue >](#)

Surfaces and Interfaces

www.elsevier.com/locate/surfin

Editors

Mircea Chipara

The University of Texas Rio Grande Valley,
Edinburg, TX 78539, USA

Hong Deng

South China University of Technology School of
Environment and Energy

Jinwei Gao

South China Normal University, Guangzhou, China

Zhenping Qu

Dalian University of Technology, Dalian, China

Klaus Zimmer

Leibniz-Institut für Oberflächenmodifizierung,
Leipzig, Germany

Editorial Board Members

Giuseppe Compagnini

Università di Catania, Catania, Italy

Serena Esposito

Politecnico di Torino,
Torino, Italy

Bronwyn Fox

Swinburne University of Technology,
Hawthorn, Victoria, Australia

Ion N. Mihailescu

National Institute for Lasers, Plasma and Radiation Physics
(INFLPR), Magurele-Bucharest, Romania

Muhd Naushad

King Saud University, Saudi Arabia

Vijay Kumar Thakur

Cranfield University, Cranfield,
England, UK

Surfaces and Interfaces

[Submit your article](#)[Menu](#)[Search in this journal](#)[Research article](#) [Full text access](#)

Temperature influence on the formation of triangular features superimposed on nanoripples produced by low-energy ion beam

Sukriti Hans, Basanta Kumar Parida, Vivek Pachchigar, Sebin Augustine, ... Mukesh Ranjan

Article 101619

[Download PDF](#) [Article preview](#)[Research article](#) [Full text access](#)

Mechanical properties and tribological performance of A356/Cr₃C₂-NiCr surface composite developed by high-velocity oxy-fuel and post friction stir processing treatment

Yousef Mazaheri, Reza Malmir, Mohammad Mahdi Jalilvand, Mohsen Sheikhi, Akbar Heidarpour

Article 101627

[Download PDF](#) [Article preview](#)[Research article](#) [Full text access](#)

Effect of carbon nanotubes additive on tribocorrosion performance of micro-arc oxidized coatings on Ti6Al4V alloy

Yufei Guo, Luyao Xu, Junji Luan, Yong Wan, Ruichuan Li

Article 101626

[Download PDF](#) [Article preview](#)[Research article](#) [Full text access](#)

The modified W₂C@C composites derived from the polyoxotungstate-based organic complexes assisted by pyrrole for efficient counter electrode in dye-sensitized solar cells

Kezhong Wu, Shan Liu, Zejin Wang, Xin Qi, ... Mingxing Wu

Article 101628

[Download PDF](#) [Article preview](#)[FEEDBACK](#)

Surfaces and Interfaces

[Submit your article](#)[Menu](#)[Search in this journal](#)[Research article](#) [Full text access](#)

Enhancement of SERS performance using hydrophobic or superhydrophobic cotton fabrics

Chao Sun, Shuo Zhang, Juan Wang, Fengyan Ge

Article 101616

[Download PDF](#) [Article preview](#)[Research article](#) [Full text access](#)

Hydrophilic nanoporous copper surface prepared by modified formic acid vapor treatment

Lap-Hong Chan, Kiyokazu Yasuda, Jenn-Ming Song, Tadatomo Suga

Article 101620

[Download PDF](#) [Article preview](#)[Research article](#) [Full text access](#)

Surface depth-dependent and microstructural analyses of high performance lithium iron silicate with 15% vanadium modification

Xiaoying Luo, Xuexia Wei, Cunhao Zhang, Jiaqi Huang, Xuan Cheng

Article 101621

[Download PDF](#) [Article preview](#)[Research article](#) [Full text access](#)

The surface and electrical properties of the Al/Ba₂P₂O₇/p-Si heterojunctions in wide range of temperature and frequency

Ömer Sevgili, Faruk Özel, Aydın Ruşen, Evin Yiğit, İkrâm Orak

Article 101637

[Download PDF](#) [Article preview](#)[Research article](#) [Full text access](#)[FEEDBACK](#)

Surfaces and Interfaces

[Submit your article](#)[Menu](#)[Search in this journal](#)[Research article](#) [Full text access](#)

Effect of UV light irradiation, pH and concentration on the dye sequestration efficiency of anionic surfactant based self-assembled aqueous mesophases

Neha Duklan, Pankaj Chamoli, K.K. Raina, Ravi K. Shukla

Article 101629

[Download PDF](#) [Article preview](#)[Research article](#) [Full text access](#)

Interfacial adhesion and surface bioactivity of anodized titanium modified with SiON and SiONP surface coatings

Kamal Awad, Simon Young, Pranesh Aswath, Venu Varanasi

Article 101645

[Download PDF](#) [Article preview](#)[Research article](#) [Full text access](#)

Formation of dense nanostructures on femtosecond laser-processed silicon carbide surfaces

Jiangyou Long, Ziyu He, Deyi Ou, Yajun Huang, ... Xiaozhu Xie

Article 101624

[Download PDF](#) [Article preview](#)[Research article](#) [Full text access](#)

Fabrication of superhydrophobic surfaces with hierarchical structure and their corrosion resistance and self-cleaning properties

Benfeng Zhu, Rujie Ou, Jiao Liu, Yumeng Yang, ... Zhao Zhang

Article 101608

[Download PDF](#) [Article preview](#)[Research article](#) [Full text access](#)[FEEDBACK](#)

Surfaces and Interfaces

[Submit your article](#)[Menu](#)[Search in this journal](#)[Research article](#) [Full text access](#)

Interfacial thermal conductance of graphene/MoS₂ heterointerface

Yang Liu, Wenhao Wu, Shixian Yang, Ping Yang

Article 101640

[Download PDF](#) [Article preview](#)[Research article](#) [Full text access](#)

Bi⁰ and oxygen vacancies co-induced enhanced visible-light photocatalytic detoxication of three typical contaminants over Bi₂WO₆ treated by NaBH₄ solution

Xingyun Jin, Shiyun Lei, Jiufu Chen, Junbo Zhong, ... Xiaoqian Tang

Article 101648

[Download PDF](#) [Article preview](#)[Research article](#) [Full text access](#)

Effect of zirconia nanotube coating on the hydrophilicity and mechanochemical behavior of zirconium for biomedical applications

Erfan Zal Nezhad, Masoud Sarraf, Farayi Musharavati, Fadi Jaber, ... Nazatul Liana Sukiman

Article 101623

[Download PDF](#) [Article preview](#)[Research article](#) [Full text access](#)

Dynamics of ternary-hybrid nanofluid subject to magnetic flux density and heat source or sink on a convectively heated surface

I.L. Animasaun, Se-Jin Yook, Taseer Muhammad, Alphonsa Mathew

Article 101654

[Download PDF](#) [Article preview](#)[Research article](#) [Full text access](#)[FEEDBACK](#)

Surfaces and Interfaces

[Submit your article](#)[Menu](#)[Search in this journal](#)[Research article](#) [Full text access](#)

Influence of Cu content on the phase composition and thermoelectric properties of deposited Cu-Se films

Guipeng Li, Guihong Song, Nan Wang, Fang Hu, ... Junhua Yuo

Article 101651

[Download PDF](#) [Article preview](#) [Research article](#) [Full text access](#)

Atomistic Simulation Study of the FCC and BCC Crystal-Melt Interface Stresses

Wen-Liang Lu, Hong-Tao Liang, Xiang-Ming Ma, Zi-Feng Yuan, ... Yang Yang

Article 101639

[Download PDF](#) [Article preview](#) [Research article](#) [Full text access](#)

Removal of Safranin T by a highly efficient adsorbent (*Cotinus Coggygia* leaves): Isotherms, kinetics, thermodynamics, and surface properties

Volkan Ugraskan, Birol Isik, Ozlem Yazici, Fatih Cakar

Article 101615

[Download PDF](#) [Article preview](#) [Research article](#) [Full text access](#)

Adhesion tuning of hydrogels via cross-linker for the junction of solid surfaces in dry and wet conditions

Bakhtawara, Syed Faizan, Luqman Ali Shah

Article 101659

[Download PDF](#) [Article preview](#) [Research article](#) [Full text access](#)[FEEDBACK](#)

Surfaces and Interfaces

[Submit your article](#)[Menu](#)[Search in this journal](#)[Research article](#) [Full text access](#)

Effect of ultrasonic peening on the surface properties of nano-layered CrN/CrAlN coating deposited by CAPVD method on D3 tool steel

Abbas Pak, Mina Masoudi, Hassan Elmkhah

Article 101618

[Download PDF](#) [Article preview](#)[Research article](#) [Full text access](#)

Direct visualization of kinetic reversibility of crystallization and dissolution behavior at solution growth interface of SiC in Si-Cr solvent

Kota Nakano, Shingo Maruyama, Tomohisa Kato, Yoshiyuki Yonezawa, ... Yuji Matsumoto

Article 101664

[Download PDF](#) [Article preview](#)[Research article](#) [Full text access](#)

Collection of polymer bubble as a nanoscale membrane

Man-Yu Qian, Ji-Huan He

Article 101665

[Download PDF](#) [Article preview](#)[Research article](#) [Full text access](#)

The impact of ZnO nanotube on the performance of hybrid inorganic/organic light-emitting diode as a single-mode ring-core UV waveguide

Mahdiyar Nouri Rezaie, Shahram Mohammadnejad, Shabnam Ahadzadeh

Article 101666

[Download PDF](#) [Article preview](#)[Research article](#) [Full text access](#)[FEEDBACK](#)

Surfaces and Interfaces

[Submit your article](#)[Menu](#)[Search in this journal](#)[Research article](#) [Full text access](#)

Interaction between HCHO molecule and B, Zn co-doped g-C₃N₄ surface: A DFT study

Cuiting Chen, Cuihua Zhao, Xi Zhou, Yong Shi, ... Liangyu Chen

Article 101667

[Download PDF](#) [Article preview](#)[Research article](#) [Full text access](#)

In-situ grown nanoscale p-n heterojunction of Cu₂S-TiO₂ thin film for efficient photoelectrocatalytic H₂ evolution

Satya Veer Singh, Urwashi Gupta, Sajal Biring, Bratindranath Mukherjee, Bhola N. Pal

Article 101660

[Download PDF](#) [Article preview](#)[Research article](#) [Full text access](#)

Synthesis of novel BiOBr/Bio-veins composite for photocatalytic degradation of pollutants under visible-light

Hu Zhou, Wenjia Qu, Ming Wu, Zhengqiu Yuan, ... Tiefan Huang

Article 101668

[Download PDF](#) [Article preview](#)[Research article](#) [Full text access](#)

Electronic structure transformation induced by dual-metal orbital hybridization in Re_xMn_{1-x}S₂ monolayer for hydrogen evolution reaction

Yun Shan, Tinghui Li, Lizhe Liu

Article 101671

[Download PDF](#) [Article preview](#)[Research article](#) [Full text access](#)[FEEDBACK](#)

Surfaces and Interfaces

[Submit your article](#)[Menu](#)[Search in this journal](#)[Research article](#) [Full text access](#)

Investigation of microstructure and reflectivity of thermally annealed Mo/Be and W/Be multilayer mirrors

Niranjan Kumar, Roman S. Pleshkov, Sergai A. Garakhin, Aleksey V. Nezhdanov, ... Nikolay I. Chkhalo

Article 101656

[Download PDF](#) [Article preview](#) [Research article](#) [Full text access](#)

Characteristics of MgO/PCL/PVP antibacterial nanofiber membranes produced by electrospinning technology

Ying Wang, Yuezhou Liu, Yongfang Qian, Lihua Lv, ... Yanjing Liu

Article 101661

[Download PDF](#) [Article preview](#) [Research article](#) [Full text access](#)

Modified epoxy resin with SEBS-g-MAH to fabricate crack-free and robust hydrophobic coatings on the surface of PP/SEBS matrix

Haoxuan Sun, Jun Zhang

Article 101662

[Download PDF](#) [Article preview](#) [Research article](#) [Full text access](#)

The phase-controllable crystallization induced by low pressure flashing in chloride anion doped quasi-2D hybrid perovskite thin films for blue light-emitting diodes

Lu Huang, Can Liu, Cewei Ren, Ziqi Nie, ... Linjun Wang

Article 101653

[Download PDF](#) [Article preview](#) [Research article](#) [Full text access](#)[FEEDBACK](#)

Surfaces and Interfaces

[Submit your article](#)[Menu](#)[Search in this journal](#)

Study of surface oxidation and recovery of clean MoTe_2 films

Trung T. Pham, Roshan Castelino, Alexandre Felten, Robert Sporken

Article 101681

[Download PDF](#) [Article preview](#)

Research article [Full text access](#)

Impact of surface morphology and thickness of tin selenide thin films on their optical properties

Remigijus Ivanauskas, Aiste Kuncute, Ingrida Ancutiene, Mindaugas Andrulevicius, Marius Mikolajunas

Article 101675

[Download PDF](#) [Article preview](#)

Research article [Full text access](#)

Effect of graphene oxide/hydroxyapatite nanocomposite on osteogenic differentiation and antimicrobial activity

Chingis Daulbayev, Fail Sultanov, Alina V. Korobeinyk, Mukhtar Yeleuov, ... Olzhas Daulbayev

Article 101683

[Download PDF](#) [Article preview](#)

Research article [Full text access](#)

Hydrazine electrooxidation activities of novel carbon nanotube supported Tin modified Palladium nanocatalysts

Omer Faruk Er, Ali Cavak, Adnan Aldemir, Hilal Kivrak

Article 101680

[Download PDF](#) [Article preview](#)

Research article [Full text access](#)

Chitosan/heparin layer-by-layer coatings for improving thromboresistance of polyurethane

Natalia N. Drozd, Alexey P. Lunkov, Balzhima Ts. Shagdarova, Yulia V. Zhuikova, ... Valeriya A. ...

[FEEDBACK](#)

Surfaces and Interfaces

[Submit your article](#)[Menu](#)[Search in this journal](#)

layer for efficient organic solar cells

Jeongbeom Cha, Haedam Jin, Mi Kyong Kim, Jong Hwan Park, Min Kim

Article 101669

[Download PDF](#) [Article preview](#)

Research article [Full text access](#)

Evaluation of superhydrophobicity of chemical-resistant magnetic spiky nickel nanowires grafted with silane coupling agent for highly efficient oil/water separation

Hadi Shayesteh, Reza Norouzbeigi, Ahmad Rahbar-Kelishami

Article 101685

[Download PDF](#) [Article preview](#)

Research article [Full text access](#)

Atomic layer deposition coated polymer films with enhanced high-temperature dielectric strength suitable for film capacitors

Xudong Wu, Yichen Liu, Xiaotian Lin, Enling Huang, ... Daniel Q. Tan

Article 101686

[Download PDF](#) [Article preview](#)

Research article [Full text access](#)

Green synthesis of TiO_2 nanoparticles using *Citrus limon* juice extract as a bio-capping agent for enhanced performance of dye-sensitized solar cells

Shalini Singh, Ishwar Chandra Maurya, Abhilasha Tiwari, Pankaj Srivastava, Lal Bahadur

Article 101652

[Download PDF](#) [Article preview](#)

Research article [Full text access](#)

Facile synthesis of a Gr-Ag/PIn nanocomposite as a binder free electrode for high-performance supercapacitor application

Mohd Shoeb, Mohammad Mobin, Sayed Mohammad Adnan, Ifra Ilyas Ansari, ... M Yusuf Ansari

Article 101650

[FEEDBACK](#)

Surfaces and Interfaces

[Submit your article](#)[Menu](#)[Search in this journal](#)

Article 101573

[Download PDF](#)[Article preview](#)

Research article Full text access

The UV photodetection enhancement of tailored ZnO nanorods by controlling the aspect ratio

Neda F. Nazari, Marjan Rajabi, Alireza Z. Moshfegh

Article 101682

[Download PDF](#)[Article preview](#)

Research article Full text access

Surface modification of Ag_3PO_4 using the alginate for highly active photocatalyst under visible light irradiation

Uyi Sulaeman, Yusvirza Khairullah Gandasasmita, Hartiwi Diastuti, Ponco Iswanto, ... Shu Yin

Article 101672

[Download PDF](#)[Article preview](#)

Research article Full text access

Fabrication of Ni-Mn LDH/ Co_3O_4 on carbon paper for the application in supercapacitors

Lin Ouyang, Chung-Hsuan Hsiao, Ying-Chieh Chen, Chi-Young Lee, Nyan-Hwa Tai

Article 101574

[Download PDF](#)[Article preview](#)

Research article Full text access

Suppression of V-pits formation in InGaN layer by stepped growth with annealing interval

Feng Liang, Degang Zhao, Zongshun Liu, Ping Chen, Jing Yang

Article 101691

[FEEDBACK](#)

Surfaces and Interfaces

[Submit your article](#)[Menu](#)[Search in this journal](#)[Download PDF](#)[Article preview](#) [Research article](#) [Full text access](#)

Effects of 7 MeV proton irradiation on microstructural, morphological, optical, and electrical properties of fluorine-doped tin oxide thin films

Bosco Oryema, Edward Jurua, Itani G. Madiba, Ishaq Ahmad, ... Malik Maaza

Article 101693

[Download PDF](#)[Research article](#) [Full text access](#)

Noticeably enhanced opto-electrical and photodetection performance of spray pyrolysis grown Mn:CdS nanostructured thin films for visible-light sensor applications

Z.R. Khan, M.S. Revathy, Mohd. Shkir, Aslam Khan, ... S. AlFaify

Article 101586

[Download PDF](#)[Article preview](#) [Research article](#) [Full text access](#)

Robust and self-healing superhydrophobic aluminum surface with excellent anti-icing performance

G.Y. Liu, Y. Yuan, R.J. Liao, H.Y. Xiang, ... C. Zhang

Article 101588

[Download PDF](#)[Article preview](#) [Research article](#) [Full text access](#)

Strong phonon coupling induces low thermal conductivity of one-dimensional carbon boron nanotube

Meng An, Haotian Wang, Yuejin Yuan, Dongsheng Chen, ... Xing Zhang

Article 101690

[Download PDF](#)[Article preview](#) [FEEDBACK](#)

Surfaces and Interfaces

[Submit your article](#)[Menu](#)[Search in this journal](#)[Research article](#) [Full text access](#)

Computational study of h-WO₃ surfaces as a semiconductor in water-splitting application

Zahra Hajiahmadi, Yavar T. Azar

Article 101695

[Download PDF](#) [Article preview](#)[Research article](#) [Full text access](#)

Hyaluronic acid bisphosphonates as antifouling antimicrobial coatings for PEO-modified titanium implants

Lyudmila V. Parfenova, Zulfia R. Galimshina, Guzel U. Gil'fanova, Eliza I. Alibaeva, ... Ruslan Z. Valiev

Article 101678

[Download PDF](#) [Article preview](#)[Research article](#) [Full text access](#)

Uniform Core-shell SiO₂@Sr₂CeO₄:Eu³⁺nanocomposites: Exploring multiple strategies towards flexible luminescent films and data security applications

H.S. Sudheendra, G.P. Darshan, M.K. Kokila, D.R. Lavanya, ... H. Nagabhushana

Article 101583

[Download PDF](#) [Article preview](#)[Research article](#) [Full text access](#)

Morphology control in oxygen-rich nanotubular titania for enzyme-free glucose detection

Aliakbar Saadati, Naimeh Naseri

Article 101590

[Download PDF](#) [Article preview](#)[Research article](#) [Full text access](#)[FEEDBACK](#)

Surfaces and Interfaces

[Submit your article](#)[Menu](#)[Search in this journal](#)

Surface modification of electrospun wound dressing material by Fe_2O_3 nanoparticles incorporating *Lactobacillus* strains for enhanced antimicrobial and antibiofilm activity

Fereshte Nazemi Harandi, Alireza Chackoshian Khorasani, Seyed Abbas Shojaosadati, Sameereh Hashemi-Najafabadi

Article 101592

[Download PDF](#) [Article preview](#)

Research article [Full text access](#)

High efficiency planar perovskite solar cell by surface disorder removal on mesoporous tin oxide

Huiming Luo, Jiarong Wang, Ligang Yuan, Huiling Tang, ... Keyou Yan

Article 101584

[Download PDF](#) [Article preview](#)

Research article [Full text access](#)

Study on the interface electronic properties of $\text{AlN}(0001)/\beta\text{-Ga}_2\text{O}_3(100)$

Xiaomin He, Jichao Hu, Zihan Zhang, Wanquan Liu, ... Jiaqi Meng

Article 101585

[Download PDF](#) [Article preview](#)

Research article [Full text access](#)

Magnetic crosslinked chitosan-tripolyphosphate/ $\text{MgO}/\text{Fe}_3\text{O}_4$ nanocomposite for reactive blue 19 dye removal: Optimization using desirability function approach

Ali H. Jawad, Uttam Kumar Sahu, Nur Aimi Jani, Zeid A. AlOthman, Lee D. Wilson

Article 101698

[Download PDF](#) [Article preview](#)

Research article [Full text access](#)

Three-zone model for Ti, Al co-doped ZnO films deposited by magnetron sputtering

Florian Bocchese, David Cornil, Emile Haye, Jérôme Cornil, Stéphane Lucas

[FEEDBACK](#)

Surfaces and Interfaces

[Submit your article](#)[Menu](#)[Search in this journal](#)

Article 101701

[Download PDF](#)[Article preview](#)

Research article Full text access

Enhancement of H₂ gas sensing properties of ZnO films by Mg alloying

Yutaka Adachi

Article 101597

[Download PDF](#)[Article preview](#)

Research article Full text access

Zn based hydroxyapatite based coatings deposited on a novel FeMoTaTiZr high entropy alloy used for bone implants

Mirela M. Codescu, Alina Vladescu, Victor Geanta, Ionelia Voiculescu, ... Mihai Iordoc

Article 101591

[Download PDF](#)[Article preview](#)

Research article Full text access

Evaluation of modified 316L surface properties through HAp suspended EDM process for biomedical application

Md Al-Amin, Ahmad Majdi Abdul-Rani, Masud Rana, Sri Hastuty, ... Abdullah bin Mahfouz

Article 101600

[Download PDF](#)[Article preview](#)

Research article Full text access

Low-cost and efficient hole transport materials based on 9-phenyl-9H-carbazole branch for perovskite solar cells

Yehui Wu, Zhiming Gong, Yue Jiang, Ru Wang, ... Jinwei Gao

Article 101598

[Download PDF](#)[Article preview](#) [FEEDBACK](#)

Surfaces and Interfaces

[Submit your article](#)[Menu](#)[Search in this journal](#)[Research article](#) [Full text access](#)

Additive-assisted cobalt electrodeposition as surface magnetic coating to enhance the inductance of spiral copper inductors

Dongming Zhang, Yuanming Chen, Yuanzhang Su, Yan Hong, ... Yongjie Du

Article 101603

[Download PDF](#) [Article preview](#)[Research article](#) [Full text access](#)

Adsorption of chlorine oxyanions, as water disinfectant by-products, on graphene flakes: A quantum chemical investigation

Sara M. Elgengehi, Sabry El-Taher, Khaled E. El-Kelany

Article 101601

[Download PDF](#) [Article preview](#)[Research article](#) [Full text access](#)

Exploring the influence of tin in micro-structural, magneto-optical and antimicrobial traits of nickel oxide nanoparticles

A. Aslinjensipriya, R. Sylvia Reena, R. Ragu, S. Grace Infantiya, ... S. Jerome Das

Article 101605

[Download PDF](#) [Article preview](#)[Research article](#) [Open access](#)

Highly efficient and stable PANI/TRGO nanocomposites as active materials for electrochemical detection of dopamine

Daria Minta, Zoraida González, Sonia Melendi-Espina, Grażyna Gryglewicz

Article 101606

[Download PDF](#) [Article preview](#)[FEEDBACK](#)

Surfaces and Interfaces

[Submit your article](#)[Menu](#)[Search in this journal](#)[Research article](#) [Full text access](#)

Inkjet printing high performance flexible electrodes via a graphene decorated Ag ink

Taijiang Liu, Jie Zhao, Dongxiang Luo, Zhuohui Xu, ... Junbiao Peng

Article 101609

[Download PDF](#) [Article preview](#)[Research article](#) [Full text access](#)

Enhanced bioactivity of 316L stainless steel with deposition of polypyrrole/hydroxyapatite layered hybrid coating: Orthopedic applications

Sadaf Mohandesnezhad, Mohamadreza Etminanfar, Soheil Mahdavi, Mir Saman Safavi

Article 101604

[Download PDF](#) [Article preview](#)[Research article](#) [Full text access](#)

Carboxymethyl- β -cyclodextrin as a good modifier agent for oxidation of dibenzothiophene

Mahboube Ghahramaninezhad, Ali Ahmadpour

Article 101612

[Download PDF](#) [Article preview](#)[Research article](#) [Full text access](#)

Effect of MoS₂ mass fraction on microstructure and tribological characteristics of laser clad Cu–10Al coating

Shao Lifan, Ge Yuan, Kong Dejun

Article 101599

[Download PDF](#) [Article preview](#)[Research article](#) [Full text access](#)[FEEDBACK](#)

[Submit your article](#)[Menu](#)[Search in this journal](#)[Research article](#) [Full text access](#)

Detection of nitrogenous and nitro-aromatic compound with thin gold films roughened by cold argon plasma as SERS-active substrate

Vimarsh Awasthi, Richa Goel, Padmnabh Rai, Satish Kumar Dubey

Article 101556

[Download PDF](#) [Article preview](#)

Review Articles

[Review article](#) [Full text access](#)

Recent advances in arsenene nanostructures towards prediction, properties, synthesis and applications

R. Bhuvaneswari, V. Nagarajan, R. Chandiramouli

Article 101610

[Download PDF](#) [Article preview](#) [Review article](#) [Full text access](#)

Methods of preparation of metal-doped and hybrid tungsten oxide nanoparticles for anticancer, antibacterial, and biosensing applications

Anirudh Sharma, Adesh K. Saini, Nitin Kumar, Neeraj Tejwan, ... Joydeep Das

Article 101641

[Download PDF](#) [Article preview](#) [Review article](#) [Full text access](#)

Preparation of modified zirconium-based metal-organic frameworks (Zr-MOFs) supported metals and recent application in environment: A review and perspectives

Quanxin Du, Renzhi Rao, Fukun Bi, Yang Yang, ... Xiaodong Zhang

Article 101647

[FEEDBACK](#)

Surfaces and Interfaces

[Submit your article](#)[Menu](#)[Search in this journal](#)[Download PDF](#)[Article preview](#) [Review article](#) [Open access](#)

Influence of wavelength and pulse duration on the selective laser ablation of WO_x, VO_x and MoO_x thin films.

C. Munoz-Garcia, D. Canteli, S. Lauzurica, M. Morales, ... C. Voz

Article 101613

[Download PDF](#)[Article preview](#) [Review article](#) [Full text access](#)

Recent advances in synthesis, modification, and potential application of tin oxide nanoparticles

Mohammed Ali Dheyab, Azlan Abdul Aziz, Mahmood S. Jameel, Nazila Oladzadabbasabadi

Article 101677

[Download PDF](#)[Article preview](#) [Review article](#) [Full text access](#)

A review of approaches for the design of high-performance electrocatalysts for ethanol electrooxidation

Chen Li, Ke Wang, Dong Xie

Article 101594

[Download PDF](#)[Article preview](#) [Review article](#) [Full text access](#)

Role of bi-layered CuSCN based hole transport films to realize highly efficient and stable perovskite solar cells

Muhammad Ali Tariq, Nadia Shahzad, Abdul Sattar, Muneeza Ahmad, ... Muhammad Imran Shahzad

Article 101657

[Download PDF](#)[Article preview](#) [FEEDBACK](#)

Surfaces and Interfaces

[Submit your article](#)[Menu](#)[Search in this journal](#)

Special Section on Advances in Photocatalysis - AdvPhotoCat2021

Research article Full text access

Cu/TiO₂ composite nanofibers with improved photocatalytic performance under UV and UV–visible light irradiation

Petronela Pascariu, Corneliu Cojocaru, Petrisor Samoila, Anton Airinei, ... Mirela Suchea

Article 101644

[Download PDF](#) Article preview [▼](#)



page 1 of 2

[Previous vol/issue](#)[Next vol/issue](#)

ISSN: 2468-0230

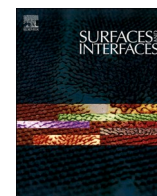
Copyright © 2022 Elsevier BV. All rights reserved



Copyright © 2022 Elsevier B.V. or its licensors or contributors.
ScienceDirect® is a registered trademark of Elsevier B.V.

RELX™

FEEDBACK



Surface modification of Ag_3PO_4 using the alginate for highly active photocatalyst under visible light irradiation

Uyi Sulaeman^{a,*}, Yusvirza Khairullah Gandasasmita^a, Hartiwi Diastuti^a, Ponco Iswanto^a, Isnaeni Isnaeni^b, Ardiansyah Taufik^c, Shu Yin^c

^a Department of Chemistry, Jenderal Soedirman University, Purwokerto 53123, Indonesia

^b Research Center for Physics, Indonesian Institute of Sciences, Building 442 Puspiptek, South Tangerang, Banten 15314, Indonesia

^c Institute of Multidisciplinary Research for Advanced Materials, Tohoku University, Sendai 980-8577, Japan

ARTICLE INFO

Keywords:

Ag_3PO_4
Alginate
Chemisorption
Conjugate
Photocatalyst

ABSTRACT

Surface modification of Ag_3PO_4 using alginate has been successfully synthesized. Ag_3PO_4 was prepared by precipitation method using CaHPO_4 /hydroxyapatite composite as a source of phosphate ion and AgNO_3 ethanol solution. Alginate was introduced on the surface of Ag_3PO_4 under the chemisorption method. Products were analyzed using XRD, DRS, PL spectra, FTIR, SEM, TEM, and XPS. A small band edge absorption at 729 nm was created after surface modification using alginate. XPS analysis showed that the binding energy shifts of 0.3 eV and 0.5 eV were observed after alginate treatment for Ag3d and P2p respectively indicating that the alginate was successfully chemically bound to the Ag_3PO_4 surface. The alginate-modified Ag_3PO_4 photocatalyst showed much higher photocatalytic activity than pure Ag_3PO_4 . The high activity is caused by the formation of conjugates that can act as electron donors under visible light irradiation.

1. Introduction

The development of Ag_3PO_4 photocatalyst is very rapid for a decade due to owing high activity under visible light exposure. The most interesting in the development of Ag_3PO_4 -based photocatalysts is the surface modification through an incorporating of elements and functional group of compounds that could improve the activity and stability of photocatalyst. This modification is very simple, cheaper, and has great challenges to provide an excellent photocatalyst.

The surface modification of Ag_3PO_4 photocatalyst can utilize an inorganic and polymer compound. The modification using inorganic compounds of ammonium phosphate [1], copper [2], tungsten [3], platinum complexes [4], and ionic liquid [5] has successfully improved the properties of Ag_3PO_4 . An ammonium phosphate can be utilized for Ag_3PO_4 surface modification resulting in a much higher photocatalytic performance for organic dye degradation under visible light irradiation [1]. Ammonium ion etching leads to a surface transition from Ag_3PO_4 to Ag^0 producing higher capture of photogenerated electrons, generating much higher $\bullet\text{O}_2^-$ radicals, whereas the adsorbed PO_4^{3-} on the Ag_3PO_4 surfaces lead to more a negative electrostatic field which enhances the holes flowing to the surface, generating much higher $\bullet\text{OH}$ radicals. The

band-gap energy of Ag_3PO_4 can also be modified using Cu under the sol-gel method [2]. The shift of the bandgap from 2.07 to 1.00 eV leads to higher activity under visible light irradiation. The incorporating tungsten (W) in Ag_3PO_4 was also successfully synthesized using the facile chemical precipitation method [3]. The W^{6+} can replace the $\text{P}^{+x002B5}$ in form of WO_4^{2-} . This approach is similar to modification using platinum complexes, where PO_4^{2-} can easily be substituted by PtCl_6^{2-} on the surface [4]. These phenomena improve catalytic activity. The ionic liquid can also be utilized to modify the surface of Ag_3PO_4 . The ionic liquid of 1-butyl-3-methylimidazole dihydrogen phosphate can increase the facet of {111} in Ag_3PO_4 surface leading to higher catalytic activity [5].

Many designs of highly active photocatalysts are organic polymers incorporated on the Ag_3PO_4 surface. The modification of Ag_3PO_4 using cyclized polyacrylonitrile (CPAN) improved the photocatalytic ability under visible light irradiation [6]. This higher activity was due to generating h^+ in the valence band of Ag_3PO_4 and $\bullet\text{O}_2^-$ radicals in the conduction band of CPAN. The polypyrrole (PPy) and multi-walled carbon nanotubes (MWCNTs) were successfully incorporated on the surface of Ag_3PO_4 [7]. This modification can bring the photogenerated holes can easily migrate to the surface of PPy, whereas the

* Corresponding author.

E-mail address: sulaeman@unsoed.ac.id (U. Sulaeman).

<https://doi.org/10.1016/j.surfin.2021.101672>

Received 19 October 2021; Received in revised form 26 November 2021; Accepted 7 December 2021

Available online 17 December 2021

2468-0230/© 2021 Elsevier B.V. All rights reserved.

photogenerated electron can easily transfer to MWCNTs, leading to high charge separation. The surface modification using a conjugated polyvinyl alcohol derivative (CDPVA) can be applied in Ag_3PO_4 using chemisorption and heat treatment [8]. This method has significantly suppressed the aggregation of particles, increased the visible-light absorbance, and resulted in more efficient separation of the electron-hole pairs. The core-shell structure of Ag_3PO_4 can be designed using a polymer of polyaniline (PANI) [9]. This modification can generate a π -conjugated structure of PANI and the hybridization effect on the surface of Ag_3PO_4 that could improve stability and activity. The energy level of PANI also matched with Ag_3PO_4 which leads to high separation of electron-hole pairs thus enhancing the photocatalytic ability. PANI shell can also inhibit the Ag_3PO_4 dissolution during the photocatalytic reaction. The polyethylene glycol (PEG) also can be used for surface modification of $\text{Ag}/\text{Ag}_2\text{O}/\text{Ag}_3\text{PO}_4/\text{Bi}_2\text{WO}_6$ composite [10]. This modification leads to small particle size, high specific surface area, and strong visible light absorption. Polydopamine (PDA) can also effectively be used to modify the surface of reduced graphene (RGO) oxide and Ag_3PO_4 to form a PDA/RGO/ Ag_3PO_4 membrane [11]. This engineered membrane enhanced the hydrophilicity properties of the surface. The hydrophilicity was induced by PDA due to a lot of oxygen-containing groups. Because of these excellent findings above, the application of the polymer in Ag_3PO_4 surface modification is very promising. Another approach, a natural polymer application to improve the properties of Ag_3PO_4 , should also be expected.

The most interesting natural polymer for photocatalyst surface modification is alginate. Alginate is one of the natural compounds that can be applied to improve the properties of photocatalysts, such as TiO_2 [12], ZnO [13], and CdS [14]. Alginate generally is derived from brown seaweed which has a structure of a linear copolymer containing a block (1,4)-linked-D-mannuronate (M) and -L-guluronate (G) residues [15]. A floating material can be designed using alginate through $\text{TiO}_2/\text{CaAlg}$ composites using the ionotropic gelation method [12]. This material can be utilized for the removal of tartrazine dye under UV-A irradiation. The floating of photocatalyst is very useful due to easy separation from a treated liquid. A core-shell structure of photocatalyst can also be designed using alginate [16]. In these cases, the floating ability can be enhanced through an internal cavity built by ice-templating. This modification improved the photocatalytic efficiency that was environmentally friendly and conveniently reclaimable. The strong interaction of alginate aerogel and TiO_2 nanoparticles through Ti-O-C was identified using XPS [17]. This interaction leads to improved electron transfer and increased photogenerated charge separation.

Up to now, there are not so many reports of alginate application in Ag_3PO_4 . Some reports are the design of $\text{CaAlg}/\text{nano-Ag}_3\text{PO}_4$ photocatalyst via in-situ synthesis [18] and Ag_3PO_4 -alginate beads [19]. The $\text{CaAlg}/\text{nano-Ag}_3\text{PO}_4$ are designed via in-situ synthesis resulting in a photocatalyst that has less flammable gas leading to application for fire protection. The Ag_3PO_4 -alginate beads can be synthesized by a simple precipitation method [19]. This material exhibited high performance for the degradation of MB and can maintain the activity to five cycles.

In this work, the surface modification using sodium alginate was demonstrated to achieve a highly active Ag_3PO_4 photocatalyst. The Ag_3PO_4 was synthesized by the precipitation method using $\text{CaHPO}_4/\text{hydroxyapatite}$ composite as source phosphate ion and silver nitrate in the ethanol solution. The single phase of Ag_3PO_4 was precipitated. Incorporating alginate on the surface of this phase significantly improved photocatalytic activity. The alginate was successful chemically bonded on the surface of Ag_3PO_4 .

2. Experimental

2.1. Synthesis of photocatalyst

The chemicals of AgNO_3 (Reag. Ph Eur, Merck), KH_2PO_4 (analytical grade, Merck), CaCl_2 (Reag. Ph Eur, Merck), NaOH (analytical grade,

Merck), and sodium alginate (Sigma-Aldrich) were used for the preparation of samples.

The photocatalyst samples were prepared using AgNO_3 and the $\text{CaHPO}_4/\text{hydroxyapatite}$ composite as a source of phosphate. To prepare the composite, the 100 mL of 1 M CaCl_2 solution was added dropwise to the 100 mL of 0.6 M KH_2PO_4 solution until white suspension formed. The pH of both solutions was adjusted at 8 using a 0.1 M NaOH solution. The suspension was aging for 12 h, then the white precipitate was separated by filtration, washed three-time and dried in an oven for 12 h at 60°C [20].

To synthesize the photocatalyst samples, firstly the ethanol solution was prepared by mixing ethanol and water at the ratio of 1:1 [21]. The AgNO_3 ethanol solution was prepared by dissolving 0.85 g of AgNO_3 into 100 mL of ethanol solution. The white $\text{CaHPO}_4/\text{hydroxyapatite}$ powder of 0.40 g was suspended into 25 mL of water. This suspension was reacted slowly (dropwise) to an AgNO_3 ethanol solution until the white suspension disappeared and changed into a yellow suspension. This yellow precipitate was separated by filtration, washed with acetone and water, dried in an oven for 12 h at 60°C . This prepared sample was named AP-H. The sample of Ag_3PO_4 which was not using $\text{CaHPO}_4/\text{hydroxyapatite}$ composite as phosphate source also prepared for photocatalytic comparison. This sample was prepared using KH_2PO_4 solution directly as a source of phosphate and the sample was named AP.

The incorporating alginate on AP-H was prepared using the chemisorption method. A certain amount of sodium alginate was dissolved into 50 mL of water. The 0.6 g AP-H were added to the alginate solution, stirred for 12 h at room temperature. The precipitate was separated using centrifugation at 1500 rpm, washed with acetone and water 3 times in beaker glass, and dried in an oven at 60°C for 4 h. The variation alginate solution was designed using 0.3 g, 0.6 g, 0.9 g, 1.2 g, 1.5 g, 1.8 g, and 2.1 g of sodium alginate which are named AP-HG03, AP-HG06, AP-HG09, AP-HG12, AP-HG15, AP-HG18, and AP-HG21, respectively.

2.2. Characterization of photocatalysts

The structures of AP, AP-H, and AP-HG15 samples were characterized using XRD (PANalytical Aeris). The XRD analysis was carried out using $\text{Cu-K}\alpha$ incident source at the range of 2θ from 5° to 80° with the step size of 0.017° . The $\text{K}\alpha_1$, $\text{K}\alpha_2$, and $\text{K}\beta$ of the light source are 1.54060 Å, 1.54443 Å, 1.39225 Å, respectively, with the $\text{K}\alpha_2/\text{K}\alpha_1$ ratio of 0.5. The diffraction patterns were refined by the Rietveld method using the HighScore Plus software. Absorption spectra of these samples and sodium alginate were investigated using UV-Vis DRS (Shimadzu UV-2450). To evaluate the separation of photogenerated electrons and holes, the photoluminescence (PL) spectra were carried out using a laser diode at 405 nm, 60 milliWatts as an excitation source. The emission was recorded by a portable MAYAPRO2000 spectrometer from Ocean Optics. The surface functional groups of samples were studied using FTIR (Shimadzu IR Prestige 21). Specific surface area, pore-volume, and pore size of these samples were also measured using the BET (Micromeritics TriStar II 3020). SEM (JEOL JSM-7800F) was utilized to investigate the morphology of AP-H and AP-HG15 samples. The AP-HG15 morphology was also investigated using TEM (ThermoFisher Talos F200X). To understand the interaction of alginate on the surface of photocatalyst, the sample of AP-H and AP-HG15 were analyzed using XPS (ULVAC PHI 5600) and the deconvolution was carried out using XPS software (XPSPEAK Version 4.1).

2.3. Photocatalysis and mechanism evaluation

The Rhodamine B (RhB) solution with the concentration of 10 mg/L was utilized as a model of wastewater for photodegradation [22]. The photocatalyst of 0.2 g was added to 250 mL of RhB solutions, stirred under a magnetic stirrer at a speed of 400 rpm. The photocatalytic evaluation was evaluated under dark and irradiated conditions for 20 min and 50 min, respectively. Blue LED was used as a source of

irradiation [4]. Samples of 4 ml were taken out from the solution every 10 min, centrifuged at 5000 rpm. The RhB concentration was measured using a spectrophotometer. To ensure the effect of alginate on the surface of photocatalyst, the photocatalytic activity was also applied to methylene blue (MB) and methyl orange (MO) photodegradation. The cyclic photocatalytic activity of AP-H and AP-HG15 were investigated for 5 cycles. The mechanism of reaction in the surface was evaluated using isopropyl alcohol (IPA), benzoquinone (BQ), and ammonium oxalate (AO) for detecting the effect of $\bullet\text{OH}$, $\bullet\text{O}_2^-$ and h^+ , respectively [23]. The red light irradiation of LED was also applied to AP-H and AP-HG15 to analyze the effect of alginate.

3. Results and discussion

3.1. Characterization of photocatalyst

The diffraction peaks of three samples were fully indexed to the cubic structure of Ag_3PO_4 , matched with the data of ICSD 98-020-1362 with the space group of P-43n (218) (Fig. 1). No other phase was observed in the XRD pattern, confirming that the structures are single phases. It is well known that a structural unit of Ag_3PO_4 is a body-centered-cubic lattice with a regular PO_4 tetrahedron [24]. The P atom is coordinated with four oxygen atoms forming the PO_4 tetrahedra and the Ag atom is surrounded by four oxygen atoms forming the AgO_4 tetrahedra, whereas the O atom is coordinated with three Ag atoms and one P atom. Three AgO_4 tetrahedra and one PO_4 tetrahedron are connected by the corner oxygen [25].

The different characteristic of the XRD profile was found in the (210) peak, shown in the insert of Fig. 1. Rietveld refinement analysis was carried to investigate the peaks (Fig. S1 in the Supplementary Material). The doublet peak of (210) was observed in the XRD profile for Ag_3PO_4 prepared using KH_2PO_4 and AgNO_3 (AP). It might be caused by the energy source of XRD that contains two lines ($\text{K}\alpha_1$ and $\text{K}\alpha_2$) with an intensity ratio of 2:1 [26]. The AP sample exhibited the angle (2θ) of 33.1909° and 33.2758° with the intensity of 4687 counts and 2343 counts for the source of $\text{K}\alpha_1$ and $\text{K}\alpha_2$, respectively. When using the composite precursor ($\text{CaHPO}_4/\text{hydroxyapatite}$), this doublet peak disappeared as shown in AP-H sample. It indicates that the preparation using the precursor of composite might cause a broadening of peak x-ray diffraction. The full width at half maximum (FWHM) of 0.0871° , 0.107° , and 0.139° was estimated for the sample of AP, AP-H, and AP-HG15, respectively (Table S1 in the Supplementary Material). The increased FWHM due to peak broadening in AP-H sample might be caused by the defect formation [27]. The defects can be created from the structural arrangement, synthetic method, and experimental conditions [28]. The alginate treatment on the surface of Ag_3PO_4 also significantly leads to a broad peak XRD shown in AP-HG15. The alginate treatment on the

sample can influence the particle size through the eroded particle on the surface. This phenomenon can lead to a broad peak of XRD. It is also well known that the peak broadening occurred in the crystal due to a crystallite smallness, micro-stresses, and chemical heterogeneities [27]. This prominent characteristic confirms that the alginate might influence the properties of Ag_3PO_4 .

The source of starting material significantly affected Ag_3PO_4 synthesis. This preparation applied the $\text{CaHPO}_4/\text{hydroxyapatite}$ as a source of phosphate ion. This starting material was obtained through the reaction of KH_2PO_4 and CaCl_2 under pH 8, resulting in white suspension of $\text{CaHPO}_4/\text{hydroxyapatite}$ composite. The XRD pattern of this composite and the reaction step formation can be seen in Fig. S2 in the Supplementary Material. It was successful that AP-H synthesized through this step resulting in a single phase of the structure. There is no CaHPO_4 or hydroxyapatite was found in the XRD pattern of AP-H, indicating the phosphate ion released from this material and creating a phase of Ag_3PO_4 . This phase could lead to a different property such as absorption and photoluminescence (PL) spectra compared to AP prepared directly with KH_2PO_4 and AgNO_3 . To make sure there is no $\text{CaHPO}_4/\text{hydroxyapatite}$, the Ca atom on the surface of Ag_3PO_4 was analyzed using high resolution of XPS (Fig. S3 in the Supplementary Material). The atomic percentage of 0.24% and 0.11% were found in the sample of AP-H and AP-HG15, respectively. After Ar^+ sputtering, the Ca content decreased to 0.14% and 0.00% for the sample of AP-H and AP-HG15, respectively. All the Ca atomic percentages are very small suggesting that the Ca-based compounds do not significantly exist.

The DRS absorptions of AP, AP-H, and AP-HG15 are displayed in Fig. 2. AP-H and AP-HG15 gave a higher absorption in the visible region above $\sim 420\text{ nm}$. This phenomenon might be related to the source of phosphate from $\text{CaHPO}_4/\text{hydroxyapatite}$ that might induce defect formation. This result was similar to the previous report that the strong absorption in the visible region was created after using the hydroxyapatite as a phosphate source in the preparation of Ag_3PO_4 [20]. It is very beneficial since the visible light responsive photocatalyst is needed to implement in sunlight irradiation, more absorption in visible light more electrons can be excited. The spectra absorptions were detail analyzed using Tauc's relation [29]. The edge absorptions at 512 nm, 521 nm, and 521 nm were found in the sample of AP, AP-H, and AP-HG15, respectively, suggesting that all samples can be well activated under blue light irradiation. The bandgap energies of 2.42 eV, 2.38 eV, and 2.38 eV were estimated for AP, AP-H, and AP-HG15, respectively (Fig. S4 in the Supplementary Material). The lower bandgap energy of AP-H and AP-HG15 might be created by different phosphate sources. The

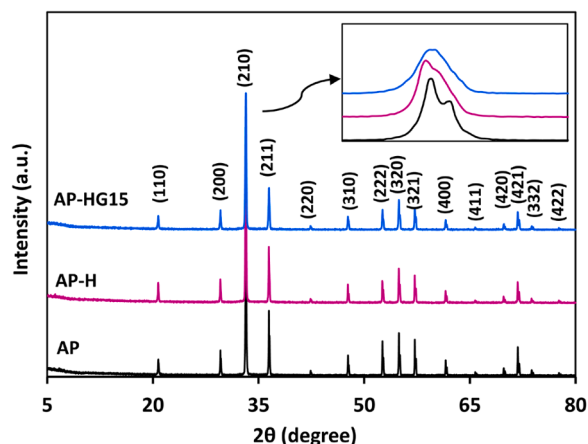


Fig. 1. XRD patterns of AP, AP-H, and AP-HG15.

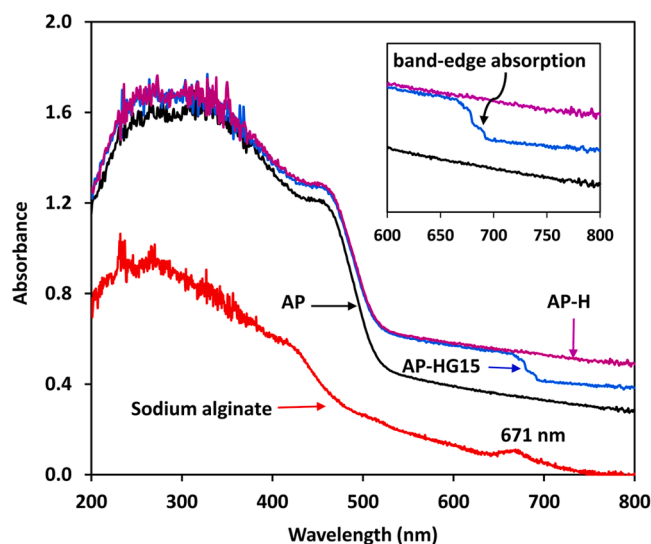


Fig. 2. Absorption spectra of AP, AP-H, AP-HG15, and sodium alginate.

incorporation of alginate on the surface of Ag_3PO_4 created a new band-edge absorption at 729 nm that can be converted to 1.70 eV of bandgap energy (insert Fig. 2). This new phenomenon in absorption might be generated by the interaction of alginate and AP-H forming a new conjugate. The sodium alginate, a material applied for the modification, was also had a small absorption at 671 nm. It might induce the new edge absorption formation of Ag_3PO_4 .

The PL spectra are very useful to assess the photogenerated charge separation of photocatalysts [30]. Fig. 3 displayed the PL spectra of AP, AP-H and AP-HG15 under the excitation wavelength of 405 nm. The PL spectra of AP exhibited high three strong emission peaks at 533, 561 and 599 nm, which were related to the recombination of photogenerated electron and hole pairs of Ag_3PO_4 . The decreased emission of AP-H, mainly in a lower wavelength of 599 nm, implies that the synthesis of Ag_3PO_4 using the composite of CaHPO_4 /hydroxyapatite as a source of phosphate ion prevents the recombination rate. It might be the defect formation in Ag_3PO_4 effectively trapping the photogenerated electron. The lowest PL spectra at 533 and 561 nm peak emissions were found in AP-HG15 indicating that the alginate effectively improves the separation of photogenerated electrons and holes.

The absorption spectra of AP, AP-H, and AP-HG15 were also investigated using FTIR ranging from 400 to 4000 cm^{-1} . All samples are similar absorption (except for the AP-HG15) as shown in Fig. 4. A broad absorption at around 3130 cm^{-1} is attributed to O—H stretching vibration, whereas the peak of 1675 cm^{-1} is attributed to H—O—H bending vibration from the water adsorbed on the surface of Ag_3PO_4 [31]. The absorption of 1080 cm^{-1} was assigned to C—O stretching [32] that might have originated from the carbon-based compound impurities. The peak of 859 cm^{-1} and 989 cm^{-1} may refer to symmetrical stretching and asymmetric stretching vibrations of P—O—P groups, respectively [33]. The strong absorption at 543 cm^{-1} was assigned to the bending vibration of O=P—O [34]. Specific vibration among the samples was found at 1032 cm^{-1} assigned to saccharide structure (C—O—C stretching) of AP-HG15 [35].

The BET surface area, pore-volume, and pore diameter of AP, AP-H and AP-HG15 were measured, and the results can be seen in Table 1. There are no significant changes in specific surface area, pore-volume, and pore diameter implying that the enhanced photocatalytic activity might not be influenced by these characteristics.

The SEM images of AP-H and AP-HG15 can be seen in Fig. 5a and b. Sphere and irregular shape with the distribution of 200–1000 nm was observed in both AP-H and AP-HG15. Carbon-based compound impurities attached to the surface were found in both AP-H and AP-HG15. The average particle sizes of 618 and 492 nm can be calculated using ImageJ processing for AP-H and AP-HG15 samples, respectively (Fig. 5c and d). The smaller particle of AP-HG15 might be induced by alginate. Small

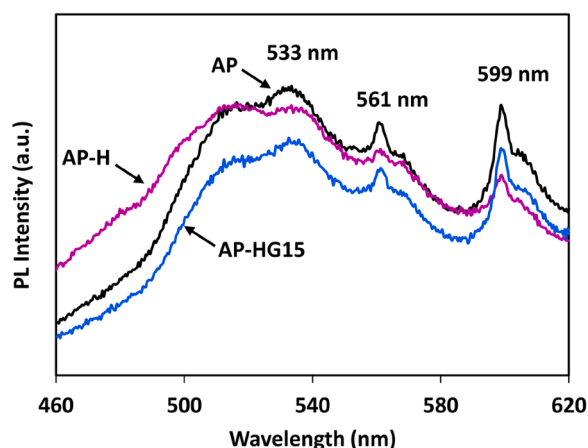


Fig. 3. PL spectra of AP, AP-H, and AP-HG15 at the excitation wavelength of 405 nm.

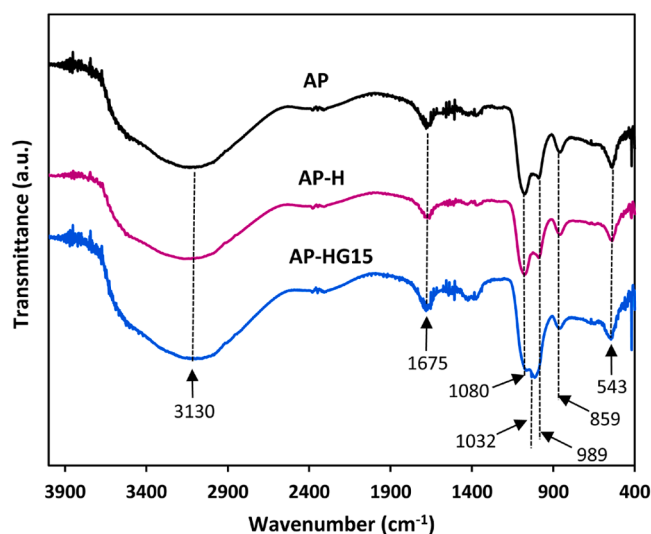


Fig. 4. FTIR spectra of AP, AP-H, and AP-HG15.

Table 1

BET surface area, pore volume, and pore diameter of AP, AP-H and AP-HG15.

| Samples | BET surface area (m^2/g) | Pore volume (cm^3/g) | Pore diameter (nm) |
|---------|--|--|--------------------|
| AP | 0.776 | 0.0036 | 18.73 |
| AP-H | 0.673 | 0.0022 | 13.17 |
| AP-HG15 | 0.901 | 0.0035 | 15.41 |

fragments can be originated from the eroded large agglomerates. Fig. 5e and f showed the several sphere particles of AP-HG15 which alginate might be chemically bonded on the surface.

3.2. XPS analysis

The effect of alginate on the surface of Ag_3PO_4 was studied using XPS. The core level of $\text{Ag}3d$, $\text{P}2p$, and $\text{O}1s$ was compared between the sample of AP-H and AP-HG15. These spectra were shown in Fig. 6. There are significant changes in binding energies (BEs) and FWHM (full-width at half-maximum) after alginate treatment. The BEs of 374.3 eV and 368.3 eV were found at peaks of $\text{Ag}3d_{3/2}$ and $\text{Ag}3d_{5/2}$, respectively for AP-H [36], these BEs decreased to 374.0 and 368.0 as found in AP-HG15. There is a shift of 0.3 eV after incorporating with alginate. The FWHM of 1.44 and 1.47 were measured at $\text{Ag}3d_{3/2}$ and $\text{Ag}3d_{5/2}$, respectively for AP-H, whereas the larger FWHM of 1.49 and 1.59 was found in AP-HG15, respectively.

To obtain detailed information, the deconvolution of $\text{P}2p$ and $\text{O}1s$ spectra were studied, the results can be seen in Fig. 7. The BEs of 134.3 eV and 133.1 eV were assigned to $\text{P}2p_{1/2}$ and $\text{P}2p_{3/2}$ respectively, found in AP-H [37]. These BEs shifted to 133.8 eV and 132.6 eV, respectively after being treated with alginate as shown in the sample of AP-HG15. There is a shift of 0.5 eV after alginate treatment. The FWHM of 1.64 eV and 1.71 eV was calculated to $\text{P}2p_{1/2}$ and $\text{P}2p_{3/2}$ of AP-H, respectively, whereas the lower FWHM of 1.59 eV and 1.54 eV was found in AP-HG15 for $\text{P}2p_{1/2}$ and $\text{P}2p_{3/2}$, respectively. From this data, the alginate treatment narrowed the $\text{P}2p$ spectra but broadened the $\text{Ag}3d$ spectra implying that alginate might be strongly attracted to these elements. The deconvolution of $\text{O}1s$ was displayed in Fig. 7c and d. The BEs of 530.9 and 532.7 eV in AP-H sample were assigned to oxygen lattice (I) and oxygen hydroxyl/organic compound (II), respectively [38]. These BEs shifted to 530.6 eV and 532.5 eV after being treated with alginate as found in the AP-HG15 sample. There is a BE shift of 0.3 eV and 0.2 eV for oxygen I and II respectively. The peak of oxygen II in AP-HG15 is higher

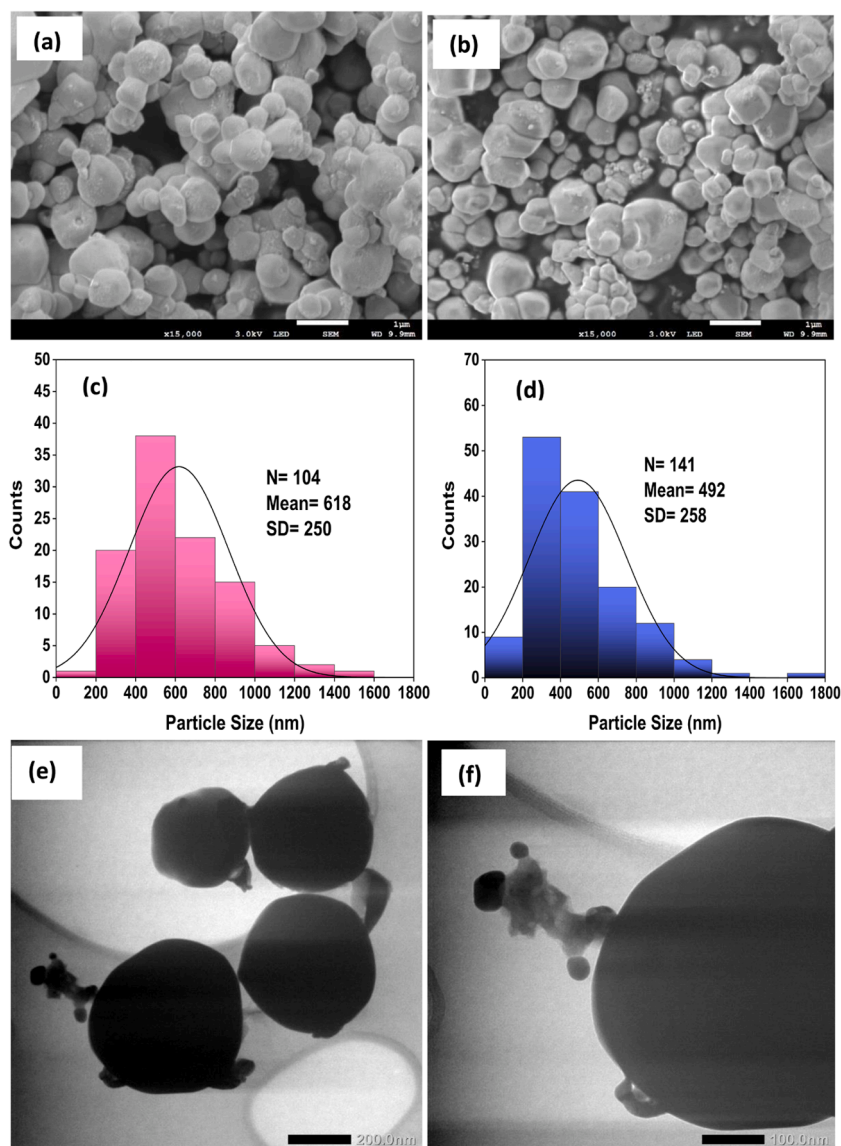


Fig. 5. SEM images of AP-H (a), AP-HG15 (b), the particle size distribution of AP-H (c), AP-HG15 (d), and TEM images of AP-HG15 (e) with higher magnification (f).

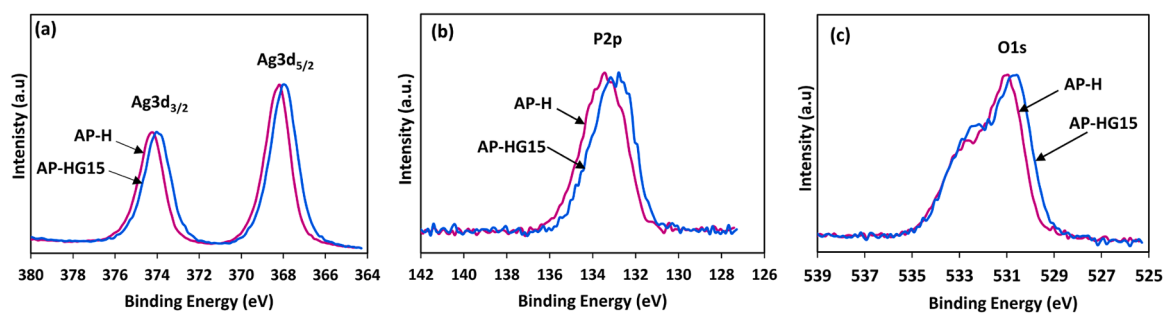


Fig. 6. XPS of Ag3d (a), P2p (b), and O1s (c) for the samples of AP-H and AP-HG15.

due to the oxygen contribution of alginate on the surface of Ag_3PO_4 .

The spectra of C1s and their deconvolution can be seen in Fig. 8. The carbon-based compound impurities were found in both AP-H and AP-HG15. The C1s spectra of AP-HG15 were larger and broader, indicating that the alginate was successfully incorporated on the surface (Fig. 8a). The alginate has remained attached on the surface after treatment with the Ar^+ sputtering as found in the sample of AP-HG15

(Fig. 8b), suggesting that alginate was strongly bonded on the surface of photocatalyst. Whereas, the carbon-based compound impurities in AP-H were completely disappeared after Ar^+ sputtering. The deconvolution of C1s AP-HG15 was displayed in Fig. 8c. The BEs of 284.6 eV, 286.2 eV, 287.3 eV, and 288.7 eV were assigned to C–C/C–H, C–O/C–O–C, C=O, and O–C=O, respectively [39]. These peaks still existed after Ar^+ sputtering, as shown in Fig. 8d.

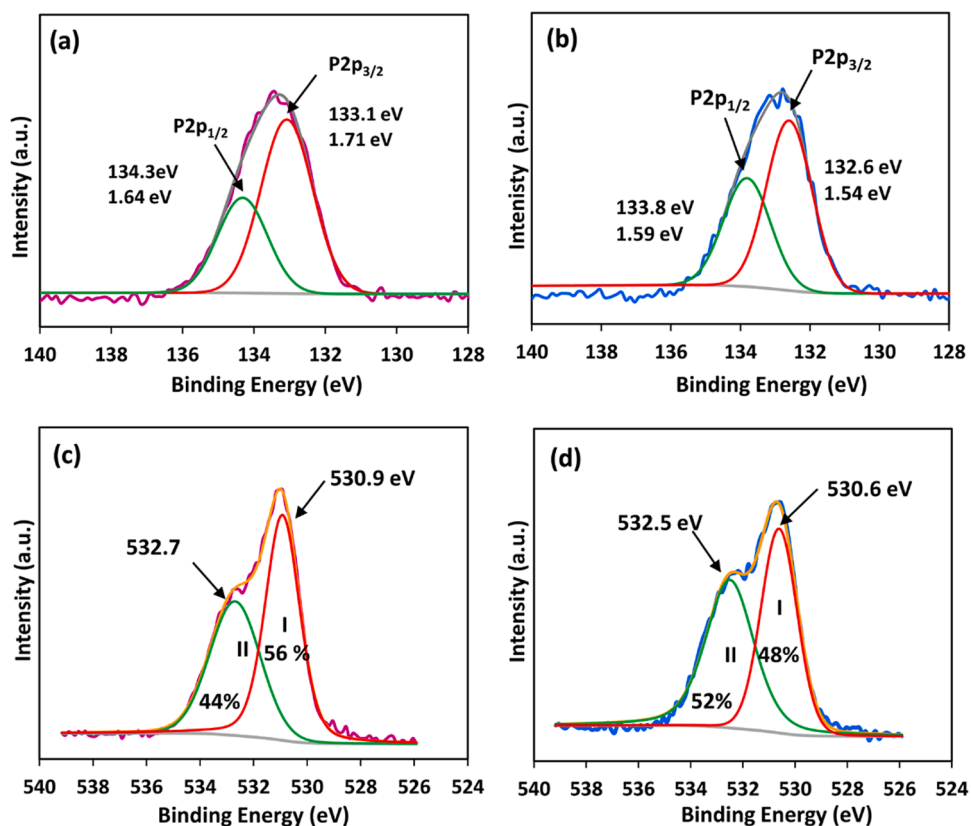


Fig. 7. XPS deconvolution of P2p AP-H (a), P2p AP-HG15 (b), O1s AP-H (c), and O1s AP-HG15 (d).

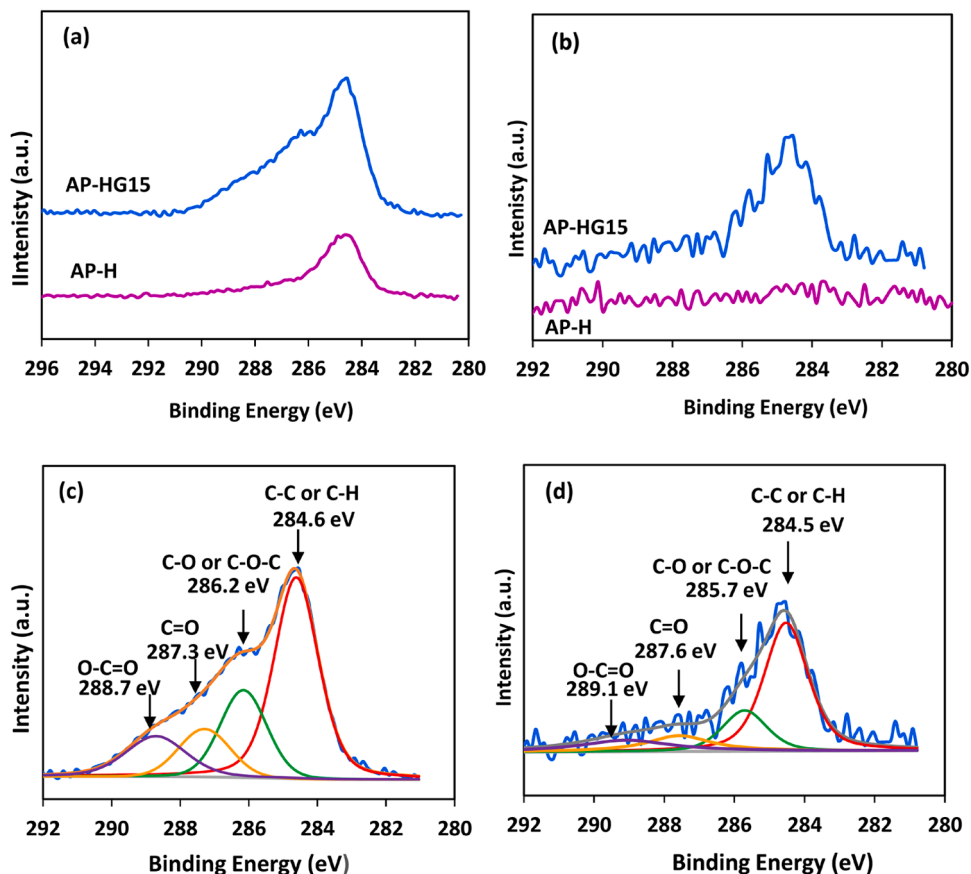


Fig. 8. C1s XPS of AP-H and AP-HG15 (a), C1s after Ar⁺ sputtering treatment (b), and C1s deconvolution of AP-HG15 (c) and after Ar⁺ sputtering treatment (d).

The Ag/P atomic ratios of 2.98 and 2.43 were found in AP-H and AP-HG15, respectively (before Ar⁺ sputtering). The lower atomic ratio of Ag/P in AP-HG15 might be caused by attaching alginate to the surface of Ag₃PO₄. A small portion of silver ion on the surface might be replaced by the functional group of alginates leading to a lower Ag⁺ content in the surface. The interaction of the alginate carboxyl group with a phosphate ion, forming the covalent bond of P–O–C. The interaction of alginate carboxyl with Ag⁺ ion might also be possible forming the ionic interaction of Ag–O–C. The chemical interaction can be illustrated in Fig. 9. These interactions lead to higher electron delocalization of alginate on the surface of Ag₃PO₄ that generates the small edge absorption at 729 nm as shown in Fig. 2. This chemical bonding can help improve the transport of charge carriers that lead to the high efficiency of the photocatalytic reaction.

The Ag/P atomic ratio of 2.86 and 3.06 was found in AP-H and AP-HG15, after Ar⁺ sputtering, respectively. The higher atomic ratio of Ag/P in AP-HG15 might be caused by the loss of phosphate ions on the surface. Since the strong covalent interaction between phosphate and carboxyl group, the phosphate ion might be swept out together with portion alginate after Ar⁺ sputtering, leading to the lower content of phosphorus in the surface of AP-HG15, therefore the atomic ratio of Ag/P increased.

3.3. Photocatalytic evaluation

The evaluation of photocatalytic activity was conducted on the samples with alginate content variation from 0.3 g to 2.1 g. The pseudo-first-order-kinetic of $\ln(C_0/C) = kt$ were applied to identify the characteristic of photocatalytic reactions [21]. C and C₀ are the RhB concentration at time t and zero respectively, k is the pseudo-first-order rate constant (min^{−1}). The results can be displayed in Fig. 10.

The average rate constants of 0.0198 min^{−1}, 0.0298 min^{−1}, 0.0545 min^{−1}, 0.0708 min^{−1}, 0.0786 min^{−1}, 0.0840 min^{−1}, 0.0909 min^{−1}, 0.0563 min^{−1} and 0.0307 min^{−1} were calculated from the sample of AP, AP-H, AP-HG03, AP-HG06, AP-HG09, AP-HG12, AP-HG15, AP-HG18, and AP-HG21, respectively. With the increase of alginate concentration, the photocatalytic activity increased and the highest activity was found at 1.5 g of alginate (AP-HG15). After more addition of alginate, the photocatalytic activity decreased. The higher alginate content on the surface of the photocatalyst might hinder the light penetration lead to decreased activity. The highest activity of AP-HG15 was found 4.6 times higher compared to the Ag₃PO₄ and 3.0 times higher compared to AP-H.

To ensure the high photocatalytic ability of AP-HG15, the comparison of AP-H and AP-HG15 was also applied to MB and MO degradation. The result can be seen in Fig. 11. For MB degradation, the rate constant of 0.010 min^{−1} was measured in a sample of AP-H and significantly increased to 0.041 min^{−1} in AP-HG15 when alginate was treated on the surface. It was 4.1 higher compared to AP-H. For MO degradation, the rate constant of 0.0057 was found in AP-H and enhanced to 0.011 in AP-HG15. It was 1.9 times higher compared to AP-H. Based on the photocatalytic tests, the alginate surface modification improves photocatalytic activity.

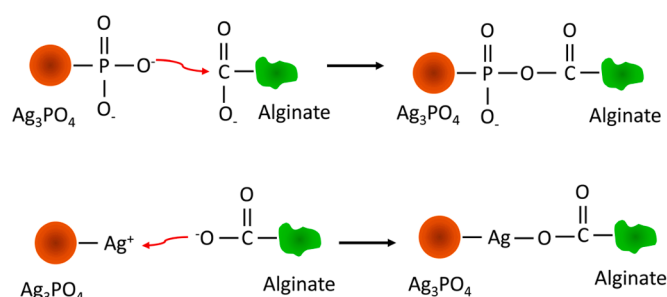


Fig. 9. The interaction of alginate on the surface of Ag₃PO₄.

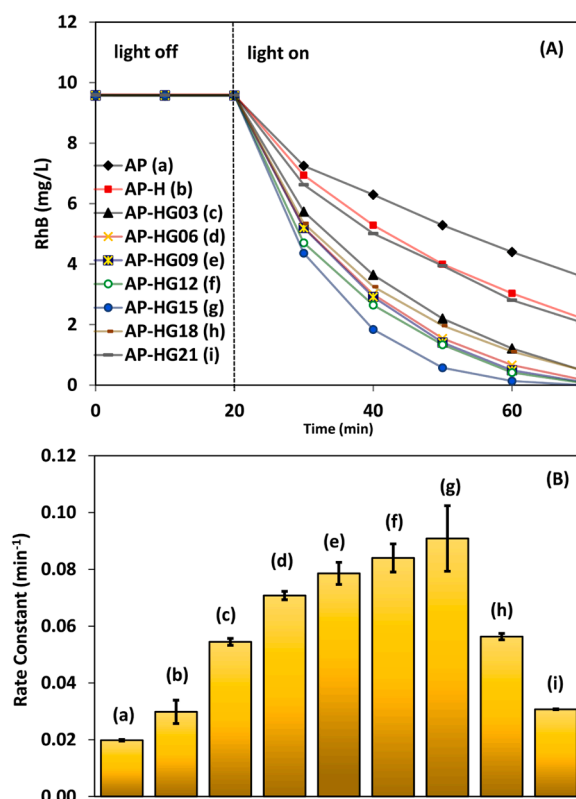


Fig. 10. The RhB photodegradation using Ag₃PO₄ photocatalyst with the variation of alginate content (0.3–2.1 gram (A), and the average rate constants of pseudo-first-order kinetic (B).

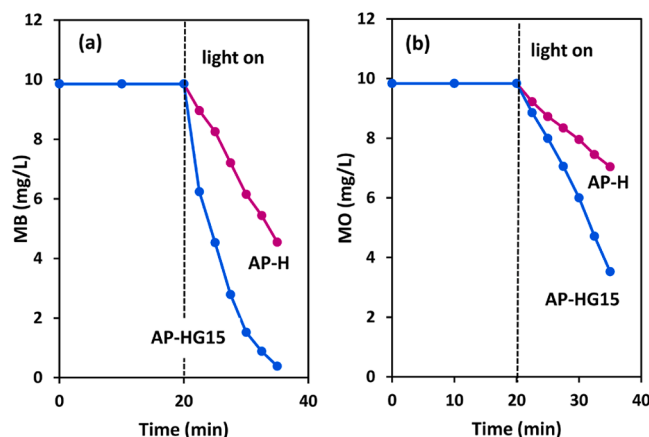


Fig. 11. The photodegradation of methylene blue (MB) (a), and methyl orange (MO) (b) using photocatalysts of AP-H and AP-HG15.

The cycle of photocatalytic activity of AP-H and AP-HG15 was also compared [Fig. 12]. The rate constant of 0.0269 min^{−1}, 0.0163 min^{−1}, 0.0078 min^{−1}, 0.0061 min^{−1}, 0.0032 min^{−1} was measured for cycle 1, cycle 2, cycle 3, cycle 4, and cycle 5 of AP-H sample, respectively. Whereas the rate constant of 0.0827 min^{−1}, 0.0449 min^{−1}, 0.0310 min^{−1}, 0.0174 min^{−1} and 0.0125 min^{−1} was obtained from cycle 1, cycle 2, cycle 3, cycle 4, and cycle 5 of AP-HG15, respectively. Every cycle of the AP-HG15 showed higher activity compared to the AP-H, indicating that the alginate-modified surface exhibited a significant effect. The gradual decrease due to the cycling test might be caused by metallic Ag formation from photo-corrosion [20,40]. The samples of AP-H and AP-HG15 after cyclic test of photocatalytic reaction were investigated

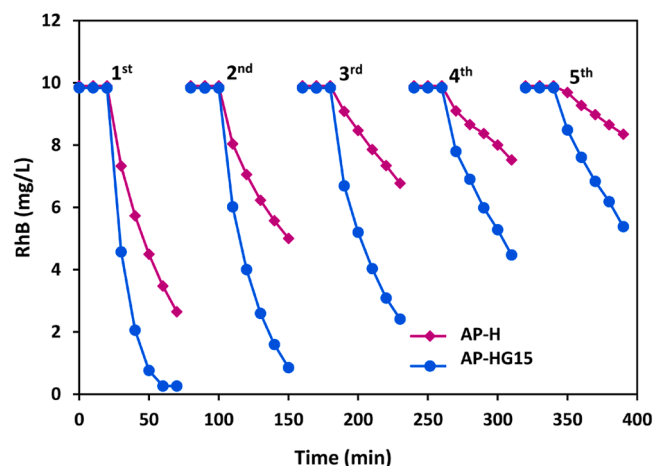


Fig. 12. The cyclic photocatalytic activity of AP-H (Ag_3PO_4 prepared without alginate) and AP-HG15 (Ag_3PO_4 prepared with alginate).

using XRD. Both AP-H and AP-HG15 exhibited a metallic Ag (Ag^0), indicating that the photoreduction occurred on the surface. The content of Ag^0 in AP-HG15 is lower than that of AP-H, suggesting that the alginate can suppress the photoreduction of Ag^+ as shown in Fig. S5 in the Supplementary Material.

3.4. Mechanism of photocatalytic reaction

The mechanism of photocatalytic activity was investigated using ammonium oxalate (AO), isopropyl alcohol (IPA), and benzoquinone (BQ) as a scavenger of holes (h^+), hydroxyl radical ($\bullet\text{OH}$), and superoxide radicals ($\text{O}_2^{\bullet-}$), respectively [23]. After the addition of scavengers, all rate constant of photocatalytic activity decreased (Fig. 13a and b). The rate constants of 0.0326 min^{-1} , 0.0213 min^{-1} , 0.0135 min^{-1} , and 0.0060 min^{-1} were calculated in AP-H for blank, IPA, BQ, and AO, respectively. Whereas the rate constant of 0.0957 min^{-1} , 0.0560 min^{-1} ,

0.0248 min^{-1} , and 0.192 min^{-1} were found in AP-HG15 for blank, IPA, BQ, and AO, respectively. The relative percentages of rate decrease in the sample can be approximated by $(k_b - k_s)/k_b \times 100\%$, where k_b is the rate constant of blank (without scavenger), k_s is the rate constant of a scavenger. The results of the photocatalytic mechanism are displayed in Fig. 13c. The relative percentages of rate decrease in AP-H were 36%, 61%, 82% for IPA, BQ, and AO, respectively, whereas in AP-HG15 sample were 41%, 74%, 80% for IPA, BQ, and AO, respectively. Both AP-H and AP-HG15 have the same order of radical role on the surface of the photocatalytic reaction, $h^+ > \text{O}_2^{\bullet-} > \bullet\text{OH}$. They have the same high h^+ role in the photocatalytic reaction. Alginate surface modification (AP-HG15) enhances the role of $\text{O}_2^{\bullet-}$ and $\bullet\text{OH}$. The increased role of $\text{O}_2^{\bullet-}$ may be due to the alginate chemical bonding on the surface of AP-HG15 which forms a new conjugate. This is supported by the absorbance feature which has a band-edge absorption at 729 nm (1.70 eV). This conjugate can act as an electron donor and promote the reduction of O_2 to $\text{O}_2^{\bullet-}$. Another radical species that increase in AP-HG15 is $\bullet\text{OH}$. The increase in $\bullet\text{OH}$ may be related to the higher phosphate ion on the surface of AP-HG15 because the ratio of Ag/P atoms in AP-HG15 is lower than that of AP-H which indicates that AP-HG15 has a large phosphate on the surface. The large negative charge of phosphate ions can maintain a large dipole that promotes photogenerated charge separation [41]. The higher negative electrostatic field created PO_3^{4-} in the surface can induce holes to flow to the surfaces and increase the formation of $\bullet\text{OH}$ radicals [1].

The visible light can excite the electron of conjugates and act as an electron donor. To ensure the mechanism, the red light with a longer wavelength of 627 nm was applied on AP-H and AP-HG15 (Fig. 13d). The results showed that there is no activity on AP-H. Surprisingly, the photocatalytic activity for RhB degradation was significantly found on the AP-HG15, indicating the conjugate molecule on the surface has a significant role in the enhancement of photocatalytic activity.

The proposed mechanism of photocatalytic reaction in the surface of AP-HG15 can be seen in Fig. 14. Upon blue light irradiation, the electron in VB can be excited into CB, producing a hole in VB which oxidizes the hydroxyl ion or water into hydroxyl radical. The conjugate molecule generated on the surface might act as a sensitizer that contributes to producing the photogenerated electron. The electron of HOMO can be excited into the LUMO of the sensitizer that directly transfers to the CB of Ag_3PO_4 . The sensitizer can act as an electron donor. This phenomenon enhances the reduction of oxygen to produce more superoxide radicals. Meanwhile, the hole formed in VB of Ag_3PO_4 might have migrated to the HOMO of conjugate increasing the separation of photogenerated electrons and holes. The HOMO directly reacts with RhB to produce the degradation products.

4. Conclusions

Alginate can effectively modify the surface of Ag_3PO_4 under the chemisorption method. Alginate treatment on the photocatalyst surface broadened the XRD peak and generated a small band-edge absorption at

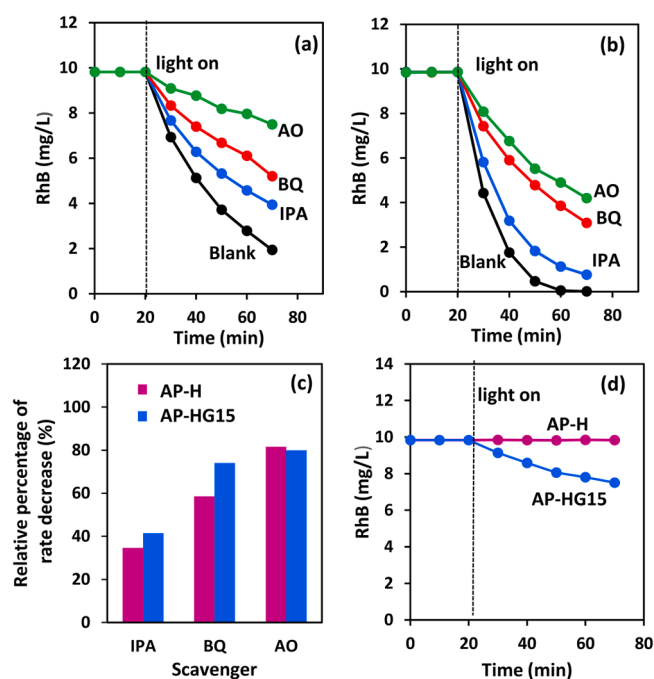


Fig. 13. The photocatalytic activity of AP-H (a), AP-HG15(b), with the variation of scavenger (IPA, BQ, AO), the relative percentage of rate decrease (c), and the effect of red light (627 nm) irradiation on the samples (d).

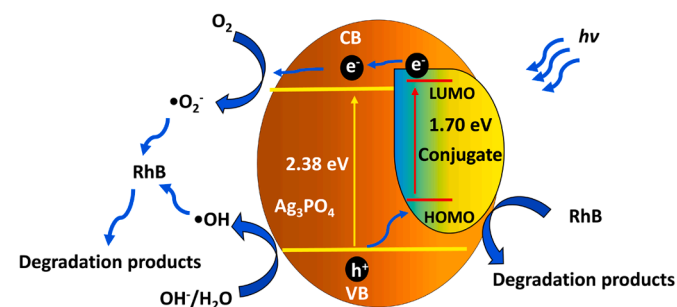


Fig. 14. Mechanism of a photocatalytic reaction on the surface of Ag_3PO_4 photocatalyst modified using alginate.

729 nm (1.70 eV). The specific 1032 cm^{-1} vibration assigned to the C–O–C stretching originates from the alginate on the surface of the photocatalyst. Lower XPS binding energy was observed due to the incorporation of alginate. Shifts of 0.3 eV and 0.5 eV were observed for Ag3d and P2p, respectively. Alginate treatment also increased the FWHM value of Ag3d and decreased the FWHM value of P2p. The different characteristics of XPS indicate that the alginate was successfully chemically bonded to the Ag_3PO_4 surface. The interaction of the alginate carboxyl group with phosphate ions can occur in the P–O–C covalent form and interaction with Ag^+ ions can occur in the Ag–O–C form. The alginate-modified Ag_3PO_4 photocatalyst has a higher photocatalytic activity under visible light irradiation. The excellent photocatalytic activity can be induced by the conjugates generated on the surface of the photocatalyst which acts as sensitizers for electron donors. This modification enhances the role of $\text{O}_2^{\bullet-}$ and $\bullet\text{OH}$ on the surface of the photocatalytic reaction.

Supporting information

Supplementary Material

CRediT authorship contribution statement

Uyi Sulaeman: Conceptualization, Methodology, Funding acquisition, Project administration, Writing – original draft, Writing – review & editing. **Yusvirza Khairullah Gandasmita:** Investigation, Formal analysis. **Hartiwi Diastuti:** Data curation, Formal analysis. **Ponco Iswanto:** Software, Validation, Visualization. **Isnaeni Isnaeni:** Formal analysis. **Ardiansyah Taufik:** Formal analysis. **Shu Yin:** Resources, Supervision.

Declaration of Competing Interest

The authors declare that they have no known competing financial interests or personal relationships that could have appeared to influence the work reported in this paper.

Acknowledgement

This research was financially supported by the Directorate of Research and Community Service, Ministry of Education, Culture, Research and Technology, the Republic of Indonesia, in the Scheme of World-Class Research (117/SP2H/LT/DRPM/2021).

Supplementary materials

Supplementary material associated with this article can be found, in the online version, at [doi:10.1016/j.surfin.2021.101672](https://doi.org/10.1016/j.surfin.2021.101672).

References

- Q. Liu, N. Li, Z. Qiao, W. Li, L. Wang, S. Zhu, Z. Jing, T. Yan, The multiple promotion effects of ammonium phosphate-modified Ag_3PO_4 on photocatalytic performance, *Front. Chem.* 7 (2019) 866, <https://doi.org/10.3389/fchem.2019.00866>.
- H. El Masaoudi, I. Benabdallah, B. Jaber, M. Benaissa, Enhanced visible light photocatalytic activity of Cu^{2+} -doped Ag_3PO_4 nanoparticles, *Chem. Phys.* 545 (2021), 111133, <https://doi.org/10.1016/j.chemphys.2021.111133>.
- Y. Ma, J. Li, Y. Jin, K. Gao, H. Cai, G. Ou, The enhancement mechanism of ultra-active Ag_3PO_4 modified by tungsten and the effective degradation towards phenolic pollutants, *Chemosphere* 285 (2021), 131440, <https://doi.org/10.1016/j.chemosphere.2021.131440>.
- U. Sulaeman, R.D. Permadi, D.R. Ningsih, H. Diastuti, A. Riapanitra, S. Yin, The surface modification of Ag_3PO_4 using anionic platinum complexes for enhanced visible-light photocatalytic activity, *Mater. Lett.* 259 (2020), 126848, <https://doi.org/10.1016/j.matlet.2019.126848>.
- B. Zhang, L. Zhang, Y. Zhang, C. Liu, J. Xia, H. Li, Ionic liquid-assisted synthesis of Ag_3PO_4 spheres for boosting photodegradation activity under visible light, *Catalysts* 11 (2021) 788, <https://doi.org/10.3390/catal11070788>.
- X. Li, R. Zheng, Q. Luo, D. Wang, J. An, R. Yin, Y. Liu, D. Wu, X. Han, Cyclized polyacrylonitrile modified Ag_3PO_4 photocatalysts with enhanced photocatalytic activity under visible-light irradiation, *Appl. Surf. Sci.* 356 (2015) 941–950, <https://doi.org/10.1016/j.apsusc.2015.08.186>.
- Y. Lin, X. Wu, Y. Han, C. Yang, Y. Ma, C. Du, Q. Teng, H. Liu, Y. Zhong, Spatial separation of photogenerated carriers and enhanced photocatalytic performance on Ag_3PO_4 catalysts via coupling with PPy and MWCNTs, *Appl. Catal. B Environ.* 258 (2019), 117969, <https://doi.org/10.1016/j.apcatb.2019.117969>.
- X. Zhu, Y. Shi, Q. Luo, J. An, R. Yin, X. Li, D. Wang, High-efficiency visible-light-driven Ag_3PO_4 photocatalysts modified by conjugated polyvinyl alcohol derivatives, *Mater. Res. Express* 6 (2019), 125558, <https://doi.org/10.1088/2053-1591/ab65e5>.
- L. Liu, L. Ding, Y. Liu, W. An, S. Lin, Y. Liang, W. Cui, A stable Ag_3PO_4 @PANI core@shell hybrid: enrichment photocatalytic degradation with π - π conjugation, *Appl. Catal. B Environ.* 201 (2017) 92–104, <https://doi.org/10.1016/j.apcatb.2016.08.005>.
- Q. Ma, X. Hu, N. Liu, A. Sharma, C. Zhang, N. Kawazoe, G. Chen, Y. Yang, Polyethylene glycol (PEG)-modified $\text{Ag}/\text{Ag}_2\text{O}/\text{Ag}_3\text{PO}_4/\text{Bi}_2\text{WO}_6$ photocatalyst film with enhanced efficiency and stability under solar light, *J. Colloid Interface Sci.* 569 (2020) 101–113, <https://doi.org/10.1016/j.jcis.2020.02.064>.
- R. Zhang, Y. Cai, X. Zhu, Q. Han, T. Zhang, Y. Liu, Y. Li, A. Wang, A novel photocatalytic membrane decorated with PDA/RGO/ Ag_3PO_4 for catalytic dye decomposition, *Colloids Surf. A: Physicochem. Eng. Asp.* 563 (2019) 68–76, <https://doi.org/10.1016/j.colsurfa.2018.11.069>.
- I. Dalponte, B.C. de Sousa, A.L. Mathias, R.M.M. Jorge, Formulation and optimization of a novel TiO_2 /calcium alginate floating photocatalyst, *Int. J. Biol. Macromol.* 137 (2019) 992–1001, <https://doi.org/10.1016/j.ijbiomac.2019.07.020>.
- S.K. Mohamed, Sh.S. Hegazy, N.A. Abdelwahab, A.M. Ramadan, Coupled adsorption-photocatalytic degradation of crystal violet under sunlight using chemically synthesized grafted sodium alginate/ ZnO /graphene oxide composite, *Int. J. Biol. Macromol.* 108 (2018) 1185–1198, <https://doi.org/10.1016/j.ijbiomac.2017.11.028>.
- L. Wang, Z. Gao, Y. Li, H. She, J. Huang, B. Yu, Q. Wang, Photosensitization of CdS by acid red-94 modified alginate: dual ameliorative effect upon photocatalytic hydrogen evolution, *Appl. Surf. Sci.* 492 (2019) 598–606, <https://doi.org/10.1016/j.apsusc.2019.06.222>.
- K.Y. Lee, D.J. Mooney, Alginate: properties and biomedical applications, *Prog. Polym. Sci.* 37 (2012) 106–126, <https://doi.org/10.1016/j.progpolymsci.2011.06.003>.
- X.H. Huang, T. Hu, H. Bu, W.X. Li, Z.L. Li, H.J. Hu, W.Z. Chen, M.Z. Lin, Y. Li, G. B. Jiang, Transparent floatable magnetic alginate sphere used as photocatalysts carrier for improving photocatalytic efficiency and recycling convenience, *Carbohydr. Polym.* 254 (2021), 117281, <https://doi.org/10.1016/j.carbpol.2020.117281>.
- J. Dai, Q. Tian, Q. Sun, W. Wei, J. Zhuang, M. Liu, Z. Cao, W. Xie, M. Fan, TiO_2 -alginate composite aerogels as novel oil/water separation and wastewater remediation filters, *Compos. Part B Eng.* 160 (2019) 480–487, <https://doi.org/10.1016/j.compositesb.2018.12.097>.
- Q. Zhang, X. Zhang, W. Cheng, Z. Li, Q. Li, In situ-synthesis of calcium alginate nano-silver phosphate hybrid material with high flame retardant and antibacterial properties, *Int. J. Biol. Macromol.* 165 (2020) 1615–1625, <https://doi.org/10.1016/j.ijbiomac.2020.10.085>.
- K. Wanchai, Exploitation of Ag_3PO_4 impregnated alginate beads for the photocatalytic degradation of dye solution under sunlight irradiation, *Key Eng. Mater.* 751 (2017) 689–694, <https://doi.org/10.4028/www.scientific.net/KEM.751.689>.
- U. Sulaeman, S. Suhendar, H. Diastuti, A. Riapanitra, S. Yin, Design of Ag_3PO_4 for highly enhanced photocatalyst using hydroxyapatite as a source of phosphate ion, *Solid State Sci.* 86 (2018) 1–5, <https://doi.org/10.1016/j.solidstatesciences.2018.09.015>.
- U. Sulaeman, D. Hermawan, R. Andreas, A.Z. Abdullah, S. Yin, Native defects in silver orthophosphate and their effects on photocatalytic activity under visible light irradiation, *Appl. Surf. Sci.* 428 (2018) 1029–1035, <https://doi.org/10.1016/j.apsusc.2017.09.188>.
- Y. Liu, C. Liu, C. Shi, W. Sun, X. Lin, W. Shi, Y. Hong, Carbon-based quantum dots (QDs) modified ms/tz-BiVO_4 heterojunction with enhanced photocatalytic performance for water purification, *J. Alloy. Compd.* 881 (2021), 160437, <https://doi.org/10.1016/j.jallcom.2021.160437>.
- S. Li, S. Hu, W. Jiang, Y. Liu, J. Liu, Z. Wang, Synthesis of n-type TaON microspheres decorated by p-type Ag_2O with enhanced visible light photocatalytic activity, *Mol. Catal.* 435 (2017) 135–143, <https://doi.org/10.1016/j.mcat.2017.03.027>.
- H.N. Ng, C. Calvo, R. Faggiani, A new investigation of the structure of silver orthophosphate, *Acta Cryst. B* 34 (1978) 898–899, <https://doi.org/10.1107/S0567740878014570>.
- X. Ma, B. Lu, D. Li, R. Shi, C. Pan, Y. Zhu, Origin of photocatalytic activation of silver orthophosphate from first-principles, *Phys. Chem. C* 115 (2011) 4680–4687, <https://doi.org/10.1021/jp111167u>.
- F. Shi, H. Dong, Q. Liu, J. Yang, S. Ren, H. Sun, J. Xiong, Investigation and theoretical calculation of the lattice vibrational spectra of BaZrO_3 ceramic, *J. Mater. Sci. Mater. Electron.* 28 (2017) 3467–3473, <https://doi.org/10.1007/s10854-016-5944-9>.
- T. Ungár, Microstructural parameters from X-ray diffraction peak broadening, *Scr. Mater.* 51 (2004) 777–781, <https://doi.org/10.1016/j.scriptamat.2004.05.007>.

- [28] G. Botelho, J. Andres, L. Gracia, L.S. Matos, E. Longo, Photoluminescence and photocatalytic properties of Ag_3PO_4 microcrystals: an experimental and theoretical investigation, *Chempluschem* 81 (2016) 202–212, <https://doi.org/10.1002/cplu.201500485>.
- [29] M. Mishra, P. Kuppusami, T.N. Sairam, A. Singh, E. Mohandas, Effect of substrate temperature and oxygen partial pressure on microstructure and optical properties of pulsed laser deposited yttrium oxide thin films, *Appl. Surf. Sci.* 257 (2011) 7665–7670, <https://doi.org/10.1016/j.apsusc.2011.03.156>.
- [30] E. Liu, X. Lin, Y. Hong, L. Yang, B. Luo, W. Shi, J. Shi, Rational copolymerization strategy engineered C self-doped $\text{g-C}_3\text{N}_4$ for efficient and robust solar photocatalytic H_2 evolution, *Renew. Energy* 178 (2021) 757–765, <https://doi.org/10.1016/j.renene.2021.06.066>.
- [31] S. Yang, D. Zhao, H. Zhang, S. Lu, L. Chen, X. Yu, Impact of environmental conditions on the sorption behavior of Pb(II) in Na-bentonite suspensions, *J. Hazard. Mater.* 183 (2010) 632–640, <https://doi.org/10.1016/j.jhazmat.2010.07.072>.
- [32] X. Miao, X. Yue, Z. Ji, X. Shen, H. Zhou, M. Liu, K. Xu, J. Zhu, G. Zhu, L. Kong, S. A. Shah, Nitrogen-doped carbon dots decorated on $\text{g-C}_3\text{N}_4/\text{Ag}_3\text{PO}_4$ photocatalyst with improved visible light photocatalytic activity and mechanism insight, *Appl. Catal. B Environ.* 227 (2018) 459–469, <https://doi.org/10.1016/j.apcatb.2018.01.057>.
- [33] N. Nourieh, R. Nabizadeh, M.A. Faramarzi, S. Nasser, K. Yaghmaeian, B. Mahmoudi, M. Alimohammadi, M. Khoobi, Photocatalytic degradation of ketoconazole by Z-scheme $\text{Ag}_3\text{PO}_4/\text{graphene oxide}$: response surface modeling and optimization, *Environ. Sci. Pollut. Res.* 27 (2020) 250–263, <https://doi.org/10.1007/s11356-019-06812-5>.
- [34] W. Zhang, L. Zhou, J. Shi, H. Deng, Synthesis of $\text{Ag}_3\text{PO}_4/\text{G-C}_3\text{N}_4$ composite with enhanced photocatalytic performance for the photodegradation of diclofenac under visible light irradiation, *Catalysts* 8 (2) (2018) 45, <https://doi.org/10.3390/catal8020045>.
- [35] P. Sundarrajan, P. Eswaran, A. Marimuthu, L.B. Subhadra, P. Kannaiyan, One pot synthesis and characterization of alginate stabilized semiconductor nanoparticles, *Bull. Korean Chem. Soc.* 33 (2012) 3218–3224, <https://doi.org/10.5012/bkcs.2012.33.10.3218>.
- [36] Z. Liu, Y. Liu, P. Xu, Z. Ma, J. Wang, H. Yuan, Rational design of wide spectral-responsive heterostructures of Au nanorod coupled Ag_3PO_4 with enhanced photocatalytic performance, *ACS Appl. Mater. Interfaces* 9 (2017) 20620–20629, <https://doi.org/10.1021/acsami.7b06824>.
- [37] Q. Xie, Y. Li, Z. Lv, H. Zhou, X. Yang, J. Chen, H. Guo, Effective adsorption and removal of phosphate from aqueous solutions and eutrophic water by Fe-based MOFs of MIL-101, *Sci. Rep.* 7 (2017) 3316, <https://doi.org/10.1038/s41598-017-03526-x>.
- [38] R. Chong, X. Cheng, B. Wang, D. Li, Z. Chang, L. Zhang, Enhanced photocatalytic activity of Ag_3PO_4 for oxygen evolution and methylene blue degeneration: effect of calcination temperature, *Int. J. Hydrog. Energy* 41 (2016) 2575–2582, <https://doi.org/10.1016/j.ijhydene.2015.12.061>.
- [39] O. Pop-Georgievski, D. Kubies, J. Zemek, N. Neykova, R. Demianchuk, E. M. Chánová, M. Šlouf, M. Houska, F. Rypáček, Self-assembled anchor layers/polysaccharide coatings on titanium surfaces: a study of functionalization and stability, *Beilstein J. Nanotechnol.* 6 (2015) 617–631, <https://doi.org/10.3762/bjnano.6.63>.
- [40] L. Luo, Y. Li, J. Hou, Y. Yang, Visible photocatalysis and photostability of Ag_3PO_4 photocatalyst, *Appl. Surf. Sci.* 319 (2014) 332–338, <https://doi.org/10.1016/j.apsusc.2014.04.154>.
- [41] C. Pan, Y. Zhu, New type of BiPO_4 oxy-acid salt photocatalyst with high photocatalytic activity on degradation of dye, *Environ. Sci. Technol.* 44 (2010) 5570–5574, <https://doi.org/10.1021/es101223n>.